

FIG. 1. Formation energy of neutral, singly and doubly charged oxygen vacancies in  $\text{CaMnO}_3$  as a function of a) biaxial strain and c) isostatic strain. Formation energies were computed for  $\mu_{\text{O}} = -5$  eV and  $E_{\text{fermi}} = 1.1$  eV. Panels b) and d) show the evolution of the transition levels with applied biaxial and isostatic strain respectively.

the formation energy at the energetically more favorable in-plane vacancy position [8], having verified that the formation energy at the out-of-plane position follows a similar trend as a function of the charge state. We chose an oxygen chemical potential  $\mu_{\text{O}} = -5$  eV, corresponding to the situation in air [8] and a Fermi energy of 1.1 eV, which is close to the theoretical band gap of 1.35 eV. We see that the formation energy of the neutral oxygen vacancy ( $V_{\text{O}}^{\bullet\bullet}$ ,  $q=0$ ) decreases under volume expansion, as expected from the chemical pressure effect discussed above. In contrast, the singly ( $V_{\text{O}}^{\bullet}$ ,  $q=1$ ) and doubly ( $V_{\text{O}}^{\times}$ ,  $q=2$ ) charged vacancies have lower formation energies under compressive strain, with the doubly charged vacancy showing the strongest strain dependence. As a result, under the chosen conditions of chemical potential and Fermi energy, neutral vacancies form preferentially at ambient or tensile strains, singly charged vacancies for compressive strains larger than 1.5%, while doubly charged vacancies would form at compressive strains larger than the 4% considered here.

These trends are consistent with the discussion above: Formation of a neutral  $V_{\text{O}}^{\bullet\bullet}$  is accompanied by the reduction of two Mn sites adjacent to the vacancy ( $\text{Mn}^{4+} \rightarrow \text{Mn}^{3+}$ ), which increases their ionic size by  $\sim 0.115$  Å (the Shannon ionic radius of 6-coordinated  $\text{Mn}^{4+} = 0.530$  Å and that of  $\text{Mn}^{3+} = 0.645$  Å [18]). Consequently neutral oxygen vacancies are favored when the volume is expanded under tensile strain and the size increase is more easily accommodated. The reduction occurs on only one

Mn for  $V_{\text{O}}^{\bullet}$  and not at all for  $V_{\text{O}}^{\times}$ . For  $V_{\text{O}}^{\bullet}$  the tendency for volume increase is thus weaker and is counteracted by the creation of empty space at the vacancy site; for  $V_{\text{O}}^{\times}$  there is no expansion mechanism and the vacancies tend to strongly reduce the volume. We emphasize then that the usual chemical expansion associated with oxygen-vacancy formation in transition-metal oxides occurs only for neutral oxygen vacancies and is a result of the reduction of the adjacent transition-metal ions. At least in the case of  $\text{CaMnO}_3$ , the intrinsic effect of the oxygen vacancies on the lattice without an accompanying reduction reaction is in fact a contraction. The same contraction for charged vacancies was also reported for  $\text{SrTiO}_3$  [19], where the doubly-charged oxygen vacancy is stable for all values of the Fermi energy [20].

The stability of oxygen vacancies in different charge states strongly depends on the position of the Fermi energy. We illustrate this in Fig. 1b), where we show the ranges of stability of the different charge states (separated by the transition levels) as a function of biaxial strain and the position of the Fermi level. We see that for Fermi energies close to the conduction band edge of 1.35 eV (dashed horizontal line in Fig. 1b), which corresponds to a physically relevant situation, the neutral defect is stable across a wide strain range, with compressive strains close to 4% being required to stabilise the  $V_{\text{O}}^{\bullet}$  defect. Conversely, for this  $E_{\text{fermi}}$ , strong compressive strain applied to a system containing neutral oxygen vacancies would cause spontaneous charging of the vacancies and a corresponding strain compensation.

In Fig. 1c) we show the corresponding calculated formation energies as a function of isostatic, rather than biaxial, strain. Since we now control the length of all three axes, we expect the strain dependence of the vacancy formation energy to be stronger than in the biaxial case. Indeed our calculations confirm this expectation: Comparing the biaxial situation in Fig. 1a) to the isostatic one in Fig. 1c), we see the same general trends of neutral  $V_{\text{O}}^{\bullet\bullet}$  favoured under tensile strain, and charged vacancies favoured under compressive strain. We notice, however, that the strain dependence is much stronger, so that under the same conditions of  $\mu_{\text{O}}$  and  $E_{\text{fermi}}$  the charged defects become stable at smaller compressive strains of around 0.5% and 3% for the singly charged ( $V_{\text{O}}^{\bullet}$ ) and the doubly charged ( $V_{\text{O}}^{\times}$ ) vacancy respectively. The ranges of stability as a function of isostatic strain and the Fermi energy are again shown in Fig. 1d), showing that compared to the biaxial case the neutral defect is stable over a smaller range of strains, compressive isostatic strain quickly promoting the formation of charged defects. We also note that the slope of the transition levels as a function of strain is much more pronounced than for biaxial strain, indicating again the stronger coupling between strain and defect formation.

In practice, the Fermi energy of a thin film can be tuned dynamically using electrostatic gating. Injection of electrons using a field effect into a material that has formed neutral oxygen vacancies to relax tensile strain

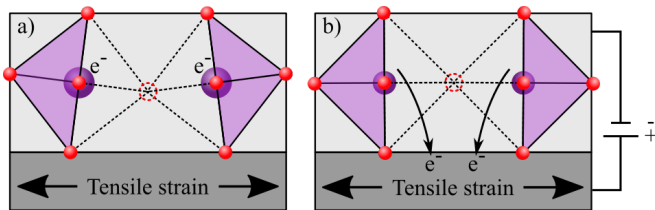


FIG. 2. a) Epitaxial film with a neutral oxygen vacancy to relax tensile strain. b) Upon gating the extra electrons are transferred to the substrate and the film changes its structure (bond lengths and angles) to accommodate the strain.

(Fig. 2a) would convert the defects from local expansion to local contraction centres, and the film would experience a renewed tensile strain. The film would then have to find other means to accommodate the strain, which we expect to happen through structural changes of the bond lengths (Fig. 2b) and angles [21]. Gating of oxygen deficient films could thus be a way to gradually and reversibly change the structure of the interfacial region and allow activation of properties induced by tensile strain such as ferroelectricity or local changes in magnetic order [22–25].

We note, however, that for a thin film in contact with a substrate, the most favourable charge state is determined in part by the band alignment between the thin film and the substrate. In Figure 3 we show two schematic band alignments between substrates and strained films. In panel a) the conduction band edge of the substrate is higher in energy than the defect state and so electrons are most favourably accommodated in the defect state

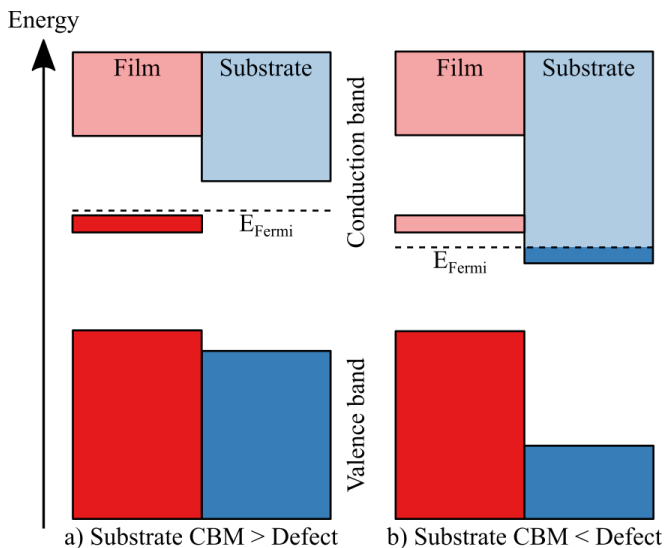


FIG. 3. Schematic illustration of the effect of the band alignment between film (red) and substrate (blue) on the charge state of the defect: a) filled defect state ( $V_O^{\bullet\bullet}$ ) when the substrate conduction-band edge is above the defect state and b) empty defect state ( $V_O^x$ ) when the substrate conduction-band edge is below the defect state.

resulting in a neutral oxygen vacancy ( $V_O^{\bullet\bullet}$ ), which readily accommodates tensile strain. In b), where the substrate conduction-band edge is at lower energy than the defect state, the electrons will tend to transfer to the substrate conduction band leaving a charged  $V_O^x$  defect that is compatible with compressive strain. While for the band alignment shown in Fig. 3a) tensile strain leads to more oxygen vacancies as we discussed above, for the band alignment shown in Fig. 3b) the opposite is true and tensile strain should in fact suppress the formation of oxygen vacancies. The choice of substrate thus not only imposes the strain, but its band alignment with the film determines the type and charge state of defects that form to accommodate the strain.

In the prototype compound  $\text{CaMnO}_3$  discussed above, the additional vacancy electrons reduce the neighboring  $\text{Mn}^{4+}$  to high-spin  $\text{Mn}^{3+}$  increasing the ionic radius and leading to the predicted simple strain dependence. In this final section we analyze the more complicated situation found in  $\text{MnO}$ , in which the reduction effect and consequently the change in radius associated with neutral oxygen vacancy formation is much smaller. In  $\text{MnO}$  the extra charge introduced by neutral oxygen vacancy formation does not primarily localise on transition-metal sites but instead forms an F-center at the vacancy site [13]. We illustrate this in Figs. 4a) and b), where we plot the defect-state charge densities for constrained neutral  $V_O^{\bullet\bullet}$  and singly charged  $V_O^\bullet$  vacancies. The characteristic F-center behavior, in which the defect charge is primarily localised on the vacancy site with only small tails on the surrounding Mn atoms, is clear. This charge localisation reflects the difficulty of reducing  $\text{Mn}^{2+}$  cations to  $\text{Mn}^{1+}$ .

In Fig. 4c) we plot the oxygen vacancy formation energies as a function of biaxial strain under the conditions  $\mu_O = -4.58$  eV,  $E_{\text{Fermi}} = 0.8$  eV corresponding to ambient conditions [13] and a Fermi energy lower than the defect state, reflecting the typical p-type nature of  $\text{MnO}$ . We see that the neutral defect ( $V_O^{\bullet\bullet}$ ) has the highest formation energy of around 4.9 eV at 0% strain. Removing electrons results in the more favourable singly  $V_O^\bullet$  and doubly  $V_O^x$  charged defects with formation energies of around 4.7 and 4.6 eV respectively at 0% strain. We can understand this behavior straightforwardly from the electronic density of states (Fig. 4d) where we see that removing electrons increasingly depopulates the defect state at around 1.5 eV above the valence-band edge.

Returning to the relative strain dependence of the individual formation energies (which is independent of the chosen chemical potential and Fermi energy) shown in Fig. 4c), we see that the formation energy of the neutral ( $V_O^{\bullet\bullet}$ ) defect depends only weakly on the applied strain, reducing by 0.03 eV (not significant within our computational accuracy) and 0.17 eV under 4% tensile and 4% compressive strain respectively. The decrease in the formation energy of the neutral defect under compressive strain is opposite to the behavior of  $\text{CaMnO}_3$ , and confirms that vacancy-induced electrons that localize on defect sites and do not reduce the surrounding transition

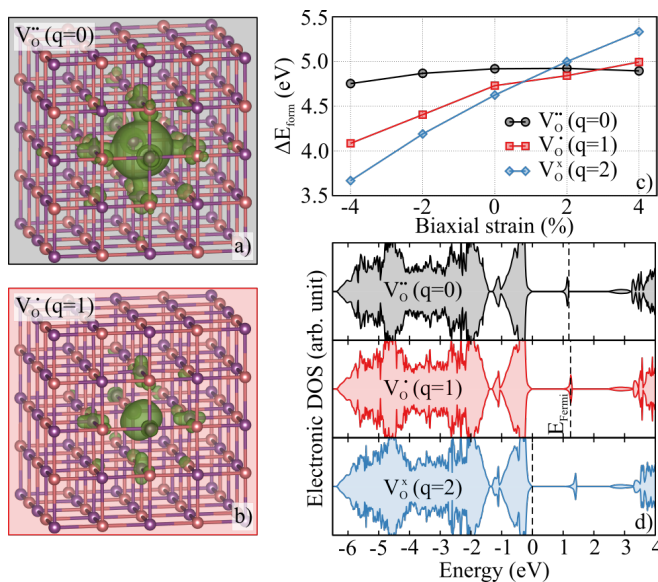


FIG. 4. Charge density associated with this defect state for a) the neutral ( $V_O^{\bullet\bullet}$ ) and b) the singly charged ( $V_O^{\bullet}$ ) defect respectively. Panel c) shows the formation energy of an oxygen vacancy in MnO in the neutral and charged states and d) the respective electronic densities of states, where the defect state about 1.5 eV above the valence-band edge is visible.

metal cations do not cause a lattice expansion. The reduction in formation energy with compressive strain for the charged defects ( $V_O^{\bullet}$  and  $V_O^{\times}$ ), is even stronger, for

the reasons that we discussed already above for  $\text{CaMnO}_3$ . This result shows that in certain situations, even neutral defects lower their formation energies under compressive strain. We anticipate similar behavior in metallic complex oxides, in which the excess charge is not well localised on specific cations.

In summary, we have shown that the magnitude and sign of the strain induced by defects in complex oxides depends sensitively on the charge state of the defect. Conversely, a change in the charge state of defects, which can be realized for example by using a field effect in a thin film geometry to add or remove carriers, will change the strain state and hence the properties of the material. The substrate in this case influences the response of the oxide both by imposing a strain via coherent heteroepitaxy and through the alignment of its band edge energies with the energy of the defect state. We hope that our calculations will motivate the development of thin film architectures to allow tunable and reversible changes in the strain state and consequently the functional properties of complex oxides.

#### ACKNOWLEDGEMENTS

This work was financially supported by the ETH Zürich and by the ERC Advanced Grant program, No. 291151. Computer resources were provided by the ETH Zürich (Euler cluster) and the Swiss Supercomputing Center (CSCS) under project s624.

- 
- [1] S. V. Kalinin, A. Y. Borisevich, and D. D. Fong, *ACS Nano* **6**, 10423 (2012).
- [2] S. V. Kalinin and N. A. Spaldin, *Science* **341**, 858 (2013).
- [3] N. Biškup, J. Salafranca, V. Mehta, M. P. Oxley, Y. Suzuki, S. J. Pennycook, S. T. Pantelides, and M. Varela, *Phys. Rev. Lett.* **112**, 087202 (2014).
- [4] S. Farokhipoor, C. Magén, S. Venkatesan, J. Íñiguez, C. J. M. Daumont, D. Rubi, E. Snoeck, M. Mostovoy, C. de Graaf, A. Müller, M. Döblinger, C. Scheu, and B. Noheda, *Nature* **515**, 379 (2014).
- [5] C. Becher, L. Maurel, U. Aschauer, M. Lilienblum, C. Magén, D. Meier, E. Langenberg, M. Trassin, J. Blasco, I. P. Krug, P. A. Algarabel, N. A. Spaldin, J. A. Pardo, and M. Fiebig, *Nat. Nanotechnol.* **10**, 661 (2015).
- [6] T. Grande, J. R. Tolchard, and S. M. Selbach, *Chem. Mater.* **24**, 338 (2012).
- [7] S. B. Adler, *J. Am. Ceram. Soc.* **84**, 2117 (2001).
- [8] U. Aschauer, R. Pfenninger, S. M. Selbach, T. Grande, and N. A. Spaldin, *Phys. Rev. B* **88**, 054111 (2013).
- [9] G. Kresse and J. Hafner, *Phys. Rev. B* **47**, 558 (1993).
- [10] G. Kresse and J. Hafner, *Phys. Rev. B* **49**, 14251 (1994).
- [11] G. Kresse and J. Furthmüller, *Comp. Mater. Sci.* **6**, 15 (1996).
- [12] G. Kresse and J. Furthmüller, *Phys. Rev. B* **54**, 11169 (1996).
- [13] U. Aschauer, N. Vonrüti, and N. A. Spaldin, *Phys. Rev. B* **92**, 054103 (2015).
- [14] C. Freysoldt, B. Grabowski, T. Hickel, J. Neugebauer, G. Kresse, A. Janotti, and C. G. Van de Walle, *Rev. Mod. Phys.* **86**, 253 (2014).
- [15] S. Lany and A. Zunger, *Phys. Rev. B* **78** (2008).
- [16] C. Freysoldt, J. Neugebauer, and C. G. Van de Walle, *Phys. Rev. Lett.* **102**, 016402 (2009).
- [17] C. Freysoldt, J. Neugebauer, and C. G. Van de Walle, *Phys. Status Solidi B* **248**, 1067 (2010).
- [18] R. D. Shannon, *Acta Cryst. A* **32**, 751 (1976).
- [19] D. S. Aidhy, B. Liu, Y. Zhang, and W. J. Weber, *Comp. Mater. Sci.* **99**, 298 (2015).
- [20] A. Janotti, J. B. Varley, M. Choi, and C. G. Van de Walle, *Phys. Rev. B* **90**, 085202 (2014).
- [21] J. M. Rondinelli and N. A. Spaldin, *Adv. Mater.* **23**, 3363 (2011).
- [22] S. Bhattacharjee, E. Bousquet, and P. Ghosez, *Phys. Rev. Lett.* **102**, 117602 (2009).
- [23] J. H. Lee and K. M. Rabe, *Phys. Rev. Lett.* **104**, 207204 (2010).
- [24] T. Günter, E. Bousquet, A. David, P. Boullay, P. Ghosez, W. Prellier, and M. Fiebig, *Phys. Rev. B* **85**, 214120 (2012).
- [25] D. Iuşan, K. Yamauchi, P. Barone, B. Sanyal, O. Eriksson, G. Profeta, and S. Picozzi, *Phys. Rev. B* **87**, 014403 (2013).